Biological Journal of the Linnean Society, 2022, **137**, 250–266. With 7 figures.

Constraining pterosaur launch: range of motion in the pectoral and pelvic girdles of a medium-sized ornithocheiraean pterosaur

BENJAMIN GRIFFIN[1,*], ELIZABETH MARTIN-SILVERSTONE[1], OLIVER DEMUTH[2,3], RODRIGO PÊGAS[4], COLIN PALMER[1] and EMILY RAYFIELD[1]

[1]*School of Earth Sciences, University of Bristol, Life Sciences Building, Bristol BS8 1TS, UK*
[2]*Department of Earth Sciences, University of Cambridge, Cambridge CB2 3EQ, UK*
[3]*Structure and Motion Laboratory, Department of Comparative Biomedical Sciences, The Royal Veterinary College, Hawkshead Lane, Hatfield AL9 7TA, UK*
[4]*Laboratório de Paleontologia de Vertebrados e Comportamento Animal, Universidade Federal do ABC, Alameda da Universidade, s/n, Anchieta, Anchieta, 09606-045, São Bernardo do Campo, SP, Brazil*

Received 18 March 2022; revised 27 April 2022; accepted for publication 2 May 2022

Launch is the most energetically expensive part of flight and is considered a limiting factor in the size of modern flyers. Pterosaurs reached significantly larger sizes than modern flyers and are proposed to have launched either bipedallly or quadrupedally. We investigated the ability of a medium-sized ornithocheiraean pterosaur to assume the poses required to launch bipedally or quadrupedally. We applied range of motion (ROM) mapping methodology to the pectoral and pelvic girdles to identify viable poses at varying levels of appendicular cartilage based on the extant phylogenetic bracket. The ROMs were constrained by novel triangulated minimum stretch methodology, used to identify the restraining tissue ROM. Our study indicates that a medium-sized ornithocheiraean could assume the poses required to use a quadrupedal launch and, with an additional 10° of hindlimb abduction, a bipedal launch, although further analysis is required to determine whether sufficient muscular power and leverage was available to propel the animal into the air.

ADDITIONAL KEYWORDS: biomechanics – flight – launch – palaeontology – pterosaur – range of motion.

INTRODUCTION

One of the most important constraints on vertebrate flight is the ability to launch (Alexander, 1998). Launching is the most energetically costly aspect of vertebrate flight, requiring the generation of both sufficient height to allow the flapping wings to clear the ground and the velocity needed to produce enough lift across the wings to remain airborne (Pennycuick, 1968; Rayner, 1988). Pterosaurs are the first known vertebrates to achieve powered flight, appearing in the fossil record in the Middle Triassic and surviving until the end Cretaceous (Middleton & English, 2015). They reached sizes greater than any other flying vertebrate, with the largest pterosaurs reaching estimated wingspans exceeding 10 m and body mass ≤250 kg (Witton, 2008; Henderson, 2010; Witton & Habib, 2010). These extremes have led to debate about whether the largest pterosaurs could generate sufficient lift and thrust for take-off and flight, with some doubting that the largest pterosaurs were capable of flight (Chatterjee & Templin, 2004; Sato *et al.*, 2009; Henderson, 2010).

Pterosaurs are considered in some studies to launch in the same manner as birds (Padian, 1983; Chatterjee & Templin, 2004, 2012; Padian *et al.*, 2021). As obligate bipeds, birds rely primarily on the hindlimbs to drive bipedal launch, with between 80 and 90% of the total launch impulse provided by the hindlimbs (Pennycuick, 1996; Earls, 2000). The proposed pterosaur bipedal launch sequence is generally considered to be the same as in birds, with the sole addition of a transition from a quadrupedal base stance to the bipedal launch pose (Chatterjee & Templin, 2004, 2012; Padian *et al.*, 2021).

Contrary to the bipedal launch hypothesis, it has also been proposed that to take off, large pterosaurs instead used a ‘quadrupedal launch’ mechanism,

*Corresponding author. E-mail: ben.griffin@bristol.ac.uk

using the combined power of the hindlimbs and the forelimbs to propel the body into the air (Habib, 2008; Molnar, 2009). This would result in more muscle mass being available for the launch and in boosting the launch impulse by increasing the launch stroke length (Palmer, 2015). As a result, this mechanism potentially circumvents size constraints calculated for modern birds (Pennycuick, 1996; Habib, 2008; Palmer, 2015). The proposed quadrupedal launch sequence is based on examination of other quadrupedal launchers, vampire and short-tailed bats, and an analysis of humeral vs. femoral strength by Habib (2008, 2011). This launch was also illustrated and simulated in animations by Molnar (2009). The quadrupedal launch requires the pterosaur to enter a deep crouch before pushing off with the hindlimbs, vaulting over the forelimbs, which then extend, releasing power stored in the enlarged flight muscles (Habib, 2008). It is proposed that the initial crouch acts as a countermovement, stretching the muscles and tendons of the limbs to facilitate a bigger leap (Molnar, 2009). By vaulting over the forelimbs, the hindlimbs can generate some initial forward momentum and supposedly enter the final bat-like flight pose in preparation for spreading of the wing aerofoil (Molnar, 2009). Most of the power and launch velocity, however, comes from co-opting the more heavily muscled forelimbs (Habib, 2008).

Some researchers have questioned the ability of all pterosaurs to assume the poses required for this style of launch (Padian, 1983; Bennett, 1990, 2001a; Manafzadeh & Padian, 2018). It was argued, before the acceptance of *Pteraichnus* trackways as pterosaur trace fossils (Witton, 2013), that the hindlimbs of pterosaurs do not assume a splayed posture. Instead, the splayed pose seen in fossils was claimed to be a post-mortem artefact generated by the large range of motion at the pterosaur acetabulum and the dislocation of the femur by the hindlimb anchoring of the wings following death (Bennett, 1990, 2001a). That an osteologically possible splayed pose is not assumed by living pterosaurs has also been cited as evidence against the ability of pterosaurs to adopt a 'bat-like' pose proposed for the vaulting and vault phases of quadrupedal launch, in addition to the flight pose most commonly depicted for pterosaurs (Manafzadeh & Padian, 2018).

Our understanding of the biomechanics of both launch hypotheses is limited. Furthermore, although there is trackway evidence available for landing (Mazin *et al.*, 2009), swimming (Lockley & Wright, 2003) and quadrupedal terrestrial locomotion associated with both basal and derived pterosaurs (Mazin *et al.*, 2003; Mazin & Pouech, 2020), there is no identifiable trackway evidence of the launch process. In lieu of more direct evidence, range of motion (ROM) investigations are often used to determine posture and locomotion in extinct animals (Hutson & Hutson, 2012). Range of motion investigations involve the physical articulation and manipulation of three-dimensional (3D) preserved bony elements to determine the extent of motion available (Bramwell & Whitfield, 1974; Nicolls & Russell, 1985; Hutson & Hutson, 2012; Manafzadeh & Padian, 2018). These investigations tend to rely on subjective decisions regarding the point of element dislocation, especially when attempting to account for offset by soft tissues, resulting in human error (as outlined by Manafzadeh & Padian, 2018). It is difficult to test all available poses systematically (Kambic *et al.*, 2017; Manafzadeh & Padian, 2018), with most ROM studies resorting to the examination of changes in one axis during development of the ROM, resulting in a greatly simplified ROM envelope (Hutson & Hutson, 2012). For pterosaurs, an additional complication is generally poor preservation, with few articulated partial specimens preserved in 3D and many specimens too fragile to be removed entirely from matrix, limiting the applicability of traditional ROM approaches. To mitigate some of these issues, a virtual ROM methodology termed 'ROM mapping' was developed (Manafzadeh & Padian, 2018; Manafzadeh & Gatesy, 2020), using 3D models of the bony elements to simulate ROM complexity in 3D space in multiple axes systematically (Kambic *et al.*, 2017; Manafzadeh & Padian, 2018). Owing to the use of digital models instead of the original fossils, this methodology can be carried out using models made from fragile, disarticulated and partially prepared specimens still in matrix. The ROM mapping methodology can also be used to test the effect of soft tissues on the joint (Demuth *et al.*, 2020), while still checking every possible pose objectively.

Here, we use ROM mapping to assess whether the poses proposed for bipedal and quadrupedal launch are feasible for a 5-m-wingspan ornithocheiraean pterosaur. Using a digital model based on a well-preserved ornithocheiraean specimen, we assess the ROM at the hip and the shoulder joints, including how the ROM is modified by addition of soft tissues: cartilage, ligament and muscle. By combining the information from all these variables, we can determine whether a bipedal and/or quadrupedal launch was viable in an ornithocheiraean within the constraints of its available ROM.

MATERIAL AND METHODS

Institutional abbreviations

AMNH, American Museum of Natural History, New York, NY, USA; BSP, Bayerische Staatssammlung für Paläontologie und Geologie, Munich, Germany; CMNH, Carnegie Museum, Pittsburgh, PA, USA; SMNK, Staatliches Museum für Naturkunde, Karlsruhe,

Germany; YPM, Yale University Peabody Museum of Natural History, New Haven, CT, USA.

Materials

First-hand observation of pterosaur specimens in the collections of the AMNH, YPM, CNHM, BSP and SMNK and in the literature (Dilkes, 1999; Bennett, 2001b, 2003, 2008; Fastnacht, 2005; Molnar, 2009; Costa *et al.*, 2014; Frigot, 2017) were used to inform the model and soft tissue placements (see also Supporting Information, Table S1 and Muscle and Ligament Reconstruction). As a framework for the 3D geometry of the model, we used computed tomography (CT) scans obtained in 2013 of SMNK PAL 1133, a partially complete 5-m-wingspan ornithocheiraean specimen (Unwin *et al.*, 1996; Elgin, 2014) from the Romualdo Formation of Brazil. It can be regarded as a specimen of either *Anhanguera* or *Coloborhynchus* (for more information on this taxonomic debate, see the Supporting Information - Provenance and Taxonomic Debate) but can be classified clearly as an ornithocheiraean. The scans were obtained at the µ-VIS X-Ray Imaging Centre at the University of Southampton and are available, in part, in the literature already (Martin-Silverstone, 2017; Martin-Silverstone *et al.*, 2018). The specimen is undistorted and preserved in 3D and includes a fused right scapulobcoracoid and associated humerus in addition to the right pelvis and associated femur, which are the primary elements required for the present study (for information on additional model elements, see the Supporting Information - Expanded Methods). The femoral head has been partially reconstructed with plaster, using closely related taxa.

Comparative poses

To identify the key poses for bipedal and quadrupedal launch in pterosaurs, we reviewed the available scientific literature for pose descriptions or figures with multiple views, from which joint angles could be extracted (Bramwell & Whitfield, 1974; Padian, 1983; Fastnacht, 2005; Molnar, 2009; Chatterjee & Templin, 2012; Witton, 2013; Costa *et al.*, 2014). The literature poses were recorded as *xyz* rotation axis coordinates and grouped into key poses based on the phase of the launch that was depicted. The individual coordinates for all instances of each key pose from the literature were then averaged to create averaged *xyz* rotation coordinates for each key pose. The key poses were then combined into a completed sequence of averaged launch poses (Fig. 1; Table 1). The key poses tested for the quadrupedal launch in this study were the quadrupedal base stance, the crouch, the vault and the final launch pose. For the bipedal launch, the key poses used were the quadrupedal starting pose, the bipedal stance pose and the launch pose. Although some birds include a countermovement crouching pose in their launches, it is not consistent for all birds (Earls, 2000). Furthermore, a countermovement crouching pose has not been proposed explicitly for pterosaur bipedal launch; therefore, we have omitted this possible pose from our study. We superimposed the joint angles and bone positions from each pose sequence from the bipedal and quadrupedal launch cycle onto our ROM simulations to determine whether bipedal and quadrupedal launch poses were possible, and if not, what degree of abduction or adduction of the joint was needed to shift the hypothesized pose into estimated viable ROM space.

Osteological range of motion

Models of the pectoral and pelvic girdles of SMNK PAL 1133 with no cartilaginous offset were created in Maya 2019 (Autodesk, San Rafael, CA, USA) using elements constructed from micro-CT scans (Supporting Information) in Avizo (v.8.1; ThermoFisher, formerly VSG, France) and cleaned in Geomagic (3Dsystems, Morrisville, NC, USA) (Supporting Information). These osteological models were designed to be comparable to the manual manipulation of the physical bones, wherein the articulation surfaces of the joint elements were in contact throughout the ROM. The pelvic girdle in all pterosaurs uses a simple ball-and socket-style joint, whereas the pectoral girdle has a more complex hemisellar joint. To simulate the additional translational complexity of the hemisellar joint, an additional slide control was required to allow the joint to accommodate the translational movement (see also Supporting Information, Figure S1 and Expanded Methods). Using this slide control, we added an additional rotation centre at the anterior and posterior extents of the glenoid. These models were animated following the ROM mapping methodology (Manafzadeh & Padian, 2018; Manafzadeh & Gatesy, 2020), with interpolation sampled at every 5° of rotation at each of the rotational centres. The interpolation data were extracted using the XROMM_MayaTools package (available at https://bitbucket.org/xromm/) and processed using cosine correction to remove Euler space distortion resulting from the selection of the starting (zero) pose (Manafzadeh & Gatesy, 2020) in MATLAB R2019a (Mathworks, Natwick, MA, USA). The resultant ROM maps were constructed with a criticalAlpha set to 'all-points', which encompasses all the viable points using the smallest possible single alphaShape.

Cartilaginous range of motion

Using cartilage correction factors previously reported for quails, ostriches and alligators (Holliday *et al.*, 2010),

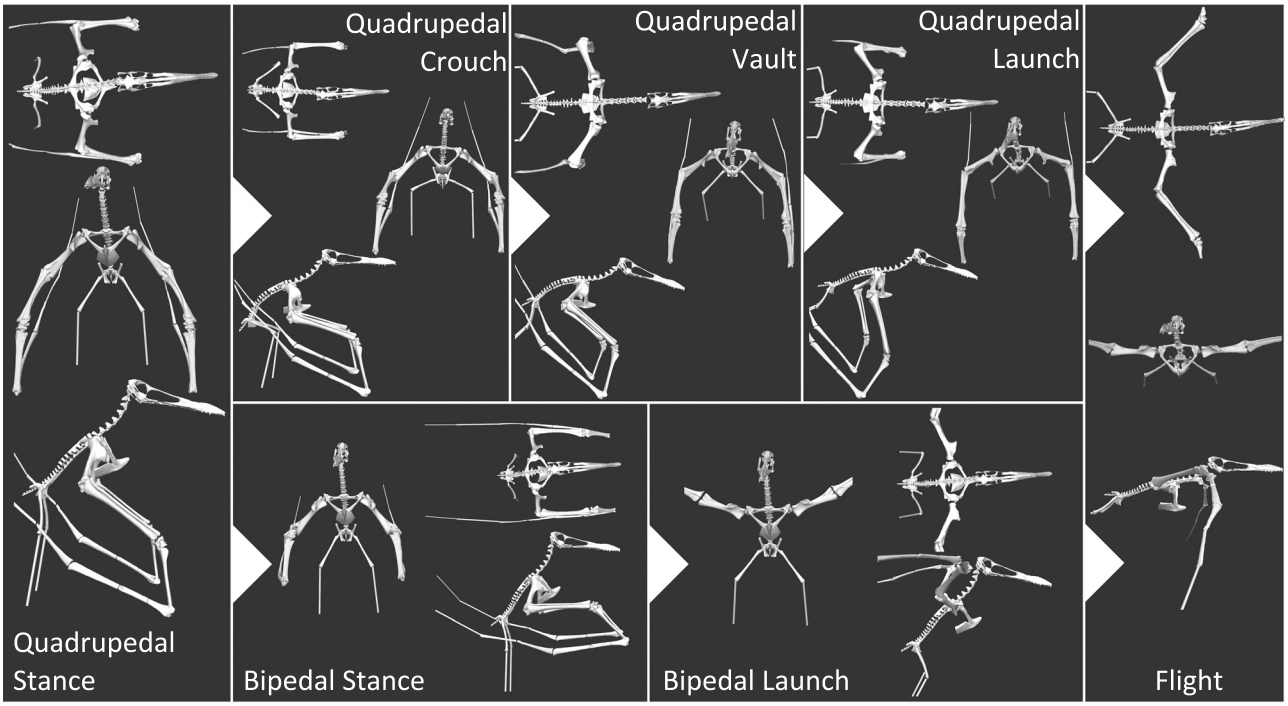

Figure 1. Comparative poses derived from the averaged joint angles presented in the literature for quadrupedal launch, flight and bipedal launch applied to our ornithocheiraean model in anterior, dorsal and lateral views (for information on model elements, see the Supporting Information - Expanded Methods).

Table 1. Averaged pose positions and coordinates relative to the joint zero pose (Supporting Information, Figure S2) for the rotating element, the humerus in the pectoral girdle and the femur in the pelvic girdle

Pose	Abduction	Flexion	Long axis rotation
Pectoral girdle			
Quadrupedal stance	−30	−30	20
Bipedal stance	−15	10	10
Bipedal launch	45	−25	0
Quadrupedal crouch	−30	5	15
Quadrupedal vault	−15	−35	20
Quadrupedal launch	−10	−40	10
Flight	0	−20	25
Pelvic girdle			
Quadrupedal stance	−60	−15	20
Bipedal stance	−75	−10	25
Bipedal launch	−75	−10	25
Quadrupedal crouch	−60	10	−5
Quadrupedal vault	−50	−10	35
Quadrupedal launch	−15	−20	10
Flight	−15	−20	10

All angles are presented in degrees.

the rotating element (humerus or femur) was offset from the osteological joint position. Three offsets were performed to simulate the different levels of cartilage offset seen using the extant phylogenetic bracket (Witmer, 1995). For the pectoral girdle, the humerus was offset by 0.8, 3.4 and 11.6 mm, and in the pelvic girdle the femur was offset by 1.4, 6.5 and 8.7 mm, based on the calculated cartilage depth corrections for quails, ostriches and alligators, respectively (Holliday *et al.*, 2010; Fig. 2). Once the offsets were applied, the ROM was calculated by following the same procedure as the osteological ROM.

Muscular/connective tissue range of motion

Muscles and ligaments constrain movement at the joint. In this third analysis, we simulated the effect of soft tissues on the estimated range of motion of the pectoral and pelvic joints. To determine which tissues (muscles or ligaments) might have constrained the joint, we studied the extant phylogenetic bracket of pterosaurs, referred to previous descriptions of joint constraint in the literature, and observed pterosaur specimens personally for evidence of muscle and ligament scars. Such preserved indicators of muscular and connective tissues in pterosaurs were examined first-hand in specimens stored in the CMNH, YPM, AMNH, SMNK and BSP collections (see also Supporting Information, Table S1 and Muscle and Ligament Reconstruction Section) and in the literature (Bennett, 2001b, 2003, 2007, 2008; Fastnacht,

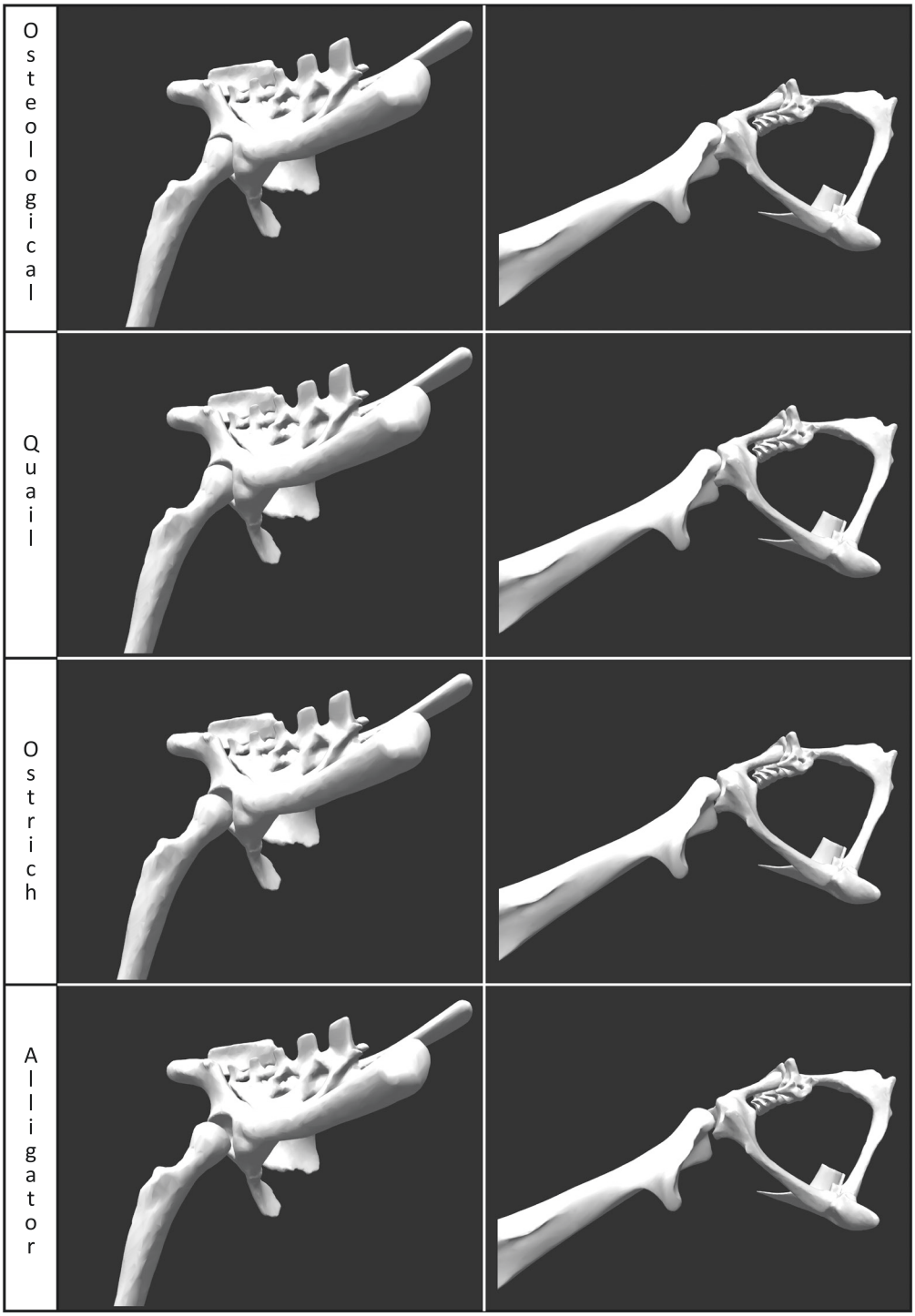

Figure 2. Pectoral and pelvic girdle models with offsets to account for different levels of cartilage offset seen in extant related taxa.

2005; Witton, 2013; Costa *et al.*, 2014). Ligaments were selected for reconstruction in the pelvic girdle because this connective tissue constrains the pelvic girdle in both birds and crocodilians in the form of a ligamentous capsule (Tsai & Holliday, 2015), and fossil evidence indicates that the pelvic girdle would also be controlled by ligaments (Manafzadeh & Padian, 2018). Owing to the conflicting naming conventions of avian and crocodilian ligaments, we followed the tetrapod inferred homology ligament names from Tsai

& Holliday (2015; Supporting Information - Muscle and Ligament Section) for the pelvic models. The pubofemoral, ischiofemoral and iliofemoral ligaments were included in our simulation.

Constraint of the pectoral girdle is more complex. In crocodilians, the pectoral girdle is constrained by the balance of muscular forces at the joint, whereas in birds the balance of forces in the pectoral girdle is controlled primarily by the ligaments (Baier *et al.*, 2007). In our simulation, we chose to use muscles to stabilize the pectoral girdle simulation. This was owing to the pterosaur joint morphology being closer to a crocodilian muscle-controlled joint morphology than the derived avian ligament-controlled joint morphology (Jenkins, 1993; Baier *et al.*, 2007). Additionally, there are only two ligaments that can be inferred confidently for the pectoral girdle based on the extant phylogenetic bracket of pterosaurs, namely the scapulohumeral and coracohumeral/acoracohumeral ligaments (P. Bishop, pers. comm.; Jenkins, 1993). We found a lack of compelling evidence for a derived avian-style acrocoracohumeral ligament in pterosaurs (Padian, 1983), wherein the ligament loops over an acrocoracoid process, in SMNK PAL 1133 and the other specimens examined during this study (Supporting Information, Table S1). As a result, the more basal crocodilian morphology of the coracohumeral ligament morphology and ROM constraint was preferred wherein the humerus is primarily constrained by the active balancing of the pectoral muscle forces (P. Bishop pers. comm.; Baier *et al.*, 2007; Hutson & Hutson, 2013). Three muscles were selected, the m. pectoralis, m. scapulohumeralis anterior and m. latissimus dorsi (Fig. 3), based on both how well defined the origin and insertion points were preserved as muscle scars and the relative importance of these muscles to locomotion (Bennett, 2003; Tokita, 2015). For detailed description of the osteological evidence for muscle and ligament attachment and insertion points, see the Supporting Information - Muscle and Ligament reconstruction.

New MAYA animated pose sequences were constructed using the subset of viable poses derived from the cartilaginous range of motion. The effect of muscles and ligaments on the joint was simulated using deformable planes referred to in the MAYA software as an "nCloth" anchored and oriented to span the longest length of the origin and insertion areas (Supporting Information - Expanded Methods; Manafzadeh & Padian, 2018). These deformable planes bend around the rigid rotating element throughout the pose sequence, in order to provide a length measurement that is more accurate than a straight point-to-point line measurement would be. The total length was measured along the centre line of the nCloth, because this is an independently derived centre of the identified attachment and origin area owing to the nCloth being automatically split into sections of equal width. The measured length is intended to be representative of the whole tissue in the same manner as a reference length, and although taking multiple length measurements from different points is possible, these would need to be averaged further to account for any selection bias and would be much more computationally expensive. These animations were designed manually to ensure animation smoothness, with each degree of freedom moving from low to high values, then back from high to low values, as opposed to returning to low values when the high values are reached as occurs in the programmatically set cartilage and osteological ROMs. In addition, to ensure animation smoothness and accuracy in the solving algorithm of the nCloth, the maximum number of iterations per step was increased to the highest value available in the version of the software used, in this case a value of 20. To accommodate for the zero position of the pose sequence, an additional 300 intermediate frames of animation were added to the start of the pectoral girdle and 150 frames to the pelvic girdle nCloth measurement animations. These frames were used for the rotating element to move gradually into the starting position of the measurement animation sequence and the subsequent normalization of the nCloth length before measurement of the nCloth began. The pectoral girdle required more animation frames to normalize owing to the additional complexity created by the slide control. Each model was run separately a minimum of three times to account for any variation in the nCloth algorithm.

As a conservative estimation of the resting lengths of the simulated muscular/connective tissues, the triangulated minimum stretch (TMS) pose was determined. This pose was found by identifying the pose with the simultaneous shortest length of all three connective tissues across the rotationally varied valid poses (see Supporting Information - Expanded Methods). By using the simultaneous shortest length across the three simulated tissues, the TMS can be identified repeatably and impartially and is not skewed by the sizes of the individual simulated tissues. The TMS pose is not intended to be an independent physiologically informative parameter; instead, the muscular/connective tissue lengths at the TMS are used as a proxy for the resting lengths for each of the tissues, in the same manner as reference lengths are used in other connective tissue studies (Hurschler *et al.*, 2003).

The ligaments and muscles were allowed to stretch during the ROM simulation, and the length data were extracted. The ROM was determined by limiting the length data values from the resting length proxy identified at the TMS pose for each soft tissue individually. The soft tissue ROM was determined after assignment of a range of stretch percentages recorded in the literature: avian acrocoracohumeral ligament, 24.5% (Baier, 2012); canine anterior cruciate

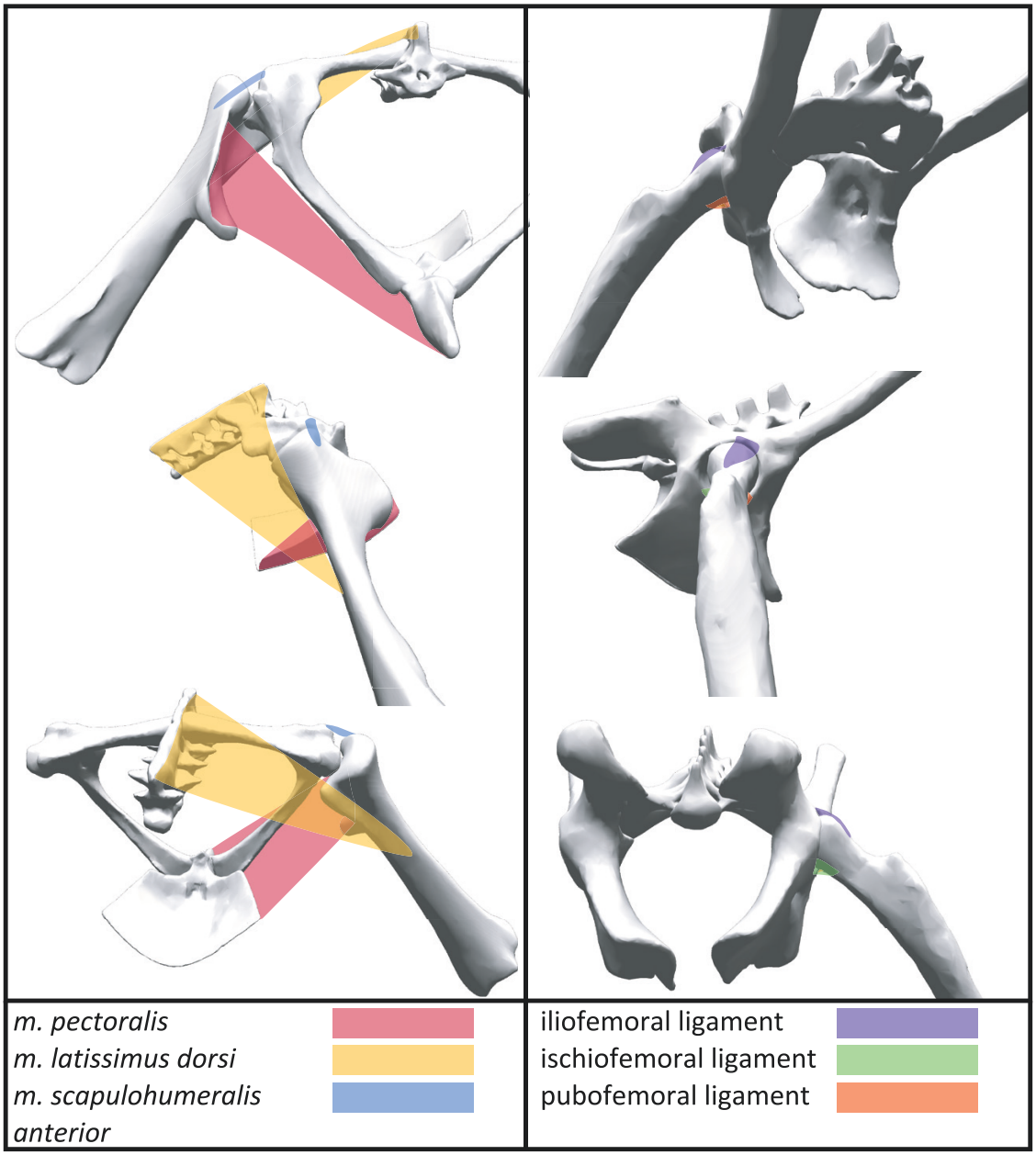

Figure 3. Soft tissues reconstructed for the study shown in anterior, lateral and posterior view. The shoulder joint in the pectoral girdle includes three muscles: the m. pectoralis, the m. latissimus dorsi and the m. scapulohumeralis anterior. The hip joint of the pelvic girdle contains three ligaments: the iliofemoral ligament, the ischiofemoral ligament and the pubofemoral ligament. All ligaments were named following the tetrapod homology convention.

ligament, 56% (Butler & Stouffer, 1983); rat medial collateral ligament, 12% (Hurschler *et al.*, 2003); rabbit medial collateral ligament, 6% at 4 months and 15% at 7 months (Liao & Belkoff, 1999); avian pectoral muscle stretch, 30–40% (Biewener, 2003); and average muscular stretch, 20–40% (Vogel, 2013). All stretch percentages were recorded to some degree of soft tissue failure, with the exception of the average muscular stretch values. The mostly high values for ligament and muscle stretch will result in a larger ROM than more restrictive values. From the TMS pose lengths, the tissue ROM was calculated by denoting each tissue length from the dataset that falls within these physiologically informative stretch percentages as a valid pose.

In order to test the validity of the TMS pose, we performed a sensitivity analysis by varying the coordinates of the TMS pose in both positive

and negative directions by 10° in each of the three rotational axes individually and in all three rotational axes simultaneously. Should the modified TMS pose fall outside of the viable cartilaginous ROM, we modified the TMS by only 5° instead, and if this also fell outside of the viable cartilaginous ROM the pose was excluded. Using these modified TMS poses, we constructed ROM maps for comparison with the unmodified TMS in both ROM map volumes. Additionally, we generated ROM maps using the animation zero pose as a replacement for the TMS pose. The zero pose, also referred to as the reference pose or starting pose, is the pose where all the translation and rotation values of the model joints are at zero (Figure S2, Demuth *et al.*, 2020). This pose is set manually during model construction and is therefore not impartial; however, it is able to be located repeatably. Only the medial centre of rotation ROM was considered when establishing the TMS pose.

RESULTS

Pectoral range of motion

Osteological range of motion

The viable poses at each of the three translational positions for the pectoral girdle were constructed and combined into a singular ROM map showing the complete joint ROM (Fig. 4). By including the maximum anterior and posterior rotational positions of the humerus in the ROM simulation, a total of 591 522 possible poses were tested, resulting in 20 308 viable poses. The inclusion of the translational humeral motion to the joint via the slide control greatly increased the viable range of motion in comparison to a stationary joint; failure to include this motion restricted the viable ROM to only 1292 poses (see also Supporting Information, Table S3). The translational ROM maps highlight that there are poses that are viable even at the low levels of muscular stretch that are not accounted for by examining the ROM simply in the medial joint pose. Within the ROM map alphaShapes, the location of the poses that corresponded to the two studied launch sequences were highlighted within the 3D space using two lines, pink for the bipedal launch sequence and purple for the quadrupedal launch. Neither of the two launch hypotheses fell within the viable poses in the osteological ROM (Fig. 4). Although the averaged launch sequences used in this study did not use the translated poses, they might be used in other motions, such as terrestrial locomotion or, potentially, aquatic launches.

Cartilage range of motion

The valid stretch poses were converted into a blue alphaShape and overlaid in the same cosine-corrected Euler space as the largest cartilage ROM alphaShape, which was presented in grey. This allowed direct comparison between the two shapes and visualization of the differences as stretch values increased. Lines indicating the position of the different poses in both launch sequences were included as with the cartilage and osteological ROM maps, and the location of the TMS pose, for reference, was also included in yellow (see also Supporting Information, Figure S4). The use of the additional rotation centres allowed by the slide control resulted in a ROM that included 24 433, 37 617 and 103 128 viable poses when introducing cartilage thicknesses seen in quail, ostrich and alligator articular cartilage, respectively. None of the hypothesized launch poses fell within the viable ROM with quail offset cartilage (the thinnest cartilage), whereas the bipedal launch pose and the flight pose were viable in the ostrich offset ROM. All the quadrupedal and bipedal launch poses fell within the viable ROM once it had been offset by the cartilage thickness equivalent to alligator, the thickest cartilage (Fig. 4).

Muscular tissue range of motion

The TMS pose in our simulation was determined to be abducted 25°, extended 70° and rotated by −135° on the longitudinal axis (see also Supporting Information, Figure S3). The number of viable poses in a connective tissue ROM with 20% muscular stretch was 1855, compared with the 103 128 poses indicated by the cartilage ROM, increasing to 23 077 poses at 30% muscle stretch and 87 435 at 40% stretch. Neither quadrupedal nor bipedal launch was fully viable at 20 or 30% muscular stretch, because the quadrupedal crouch pose and the bipedal launch pose were outside the viable pose envelope. By 40% muscle stretch, both launch motions were fully within the viable ROM (Figure 4 and Figure S5).

Pelvic range of motion

Osteological range of motion

Of the 197 174 possible poses tested, 26 406 were considered viable. The quadrupedal launch and flight poses were within the point cloud of viable poses in the osteological ROM analysis. The quadrupedal stance and crouch poses and the bipedal stance pose were not viable in the osteological ROM, falling slightly outside the envelope of the point cloud (Fig. 5).

Cartilage range of motion

When introducing a cartilage offset to levels equivalent to those seen in quails, ostriches and alligators, the range of motion increased from 26 406 valid poses (osteological ROM) to 28 607, 31 375 and 39 767 valid poses, respectively (see also Supporting

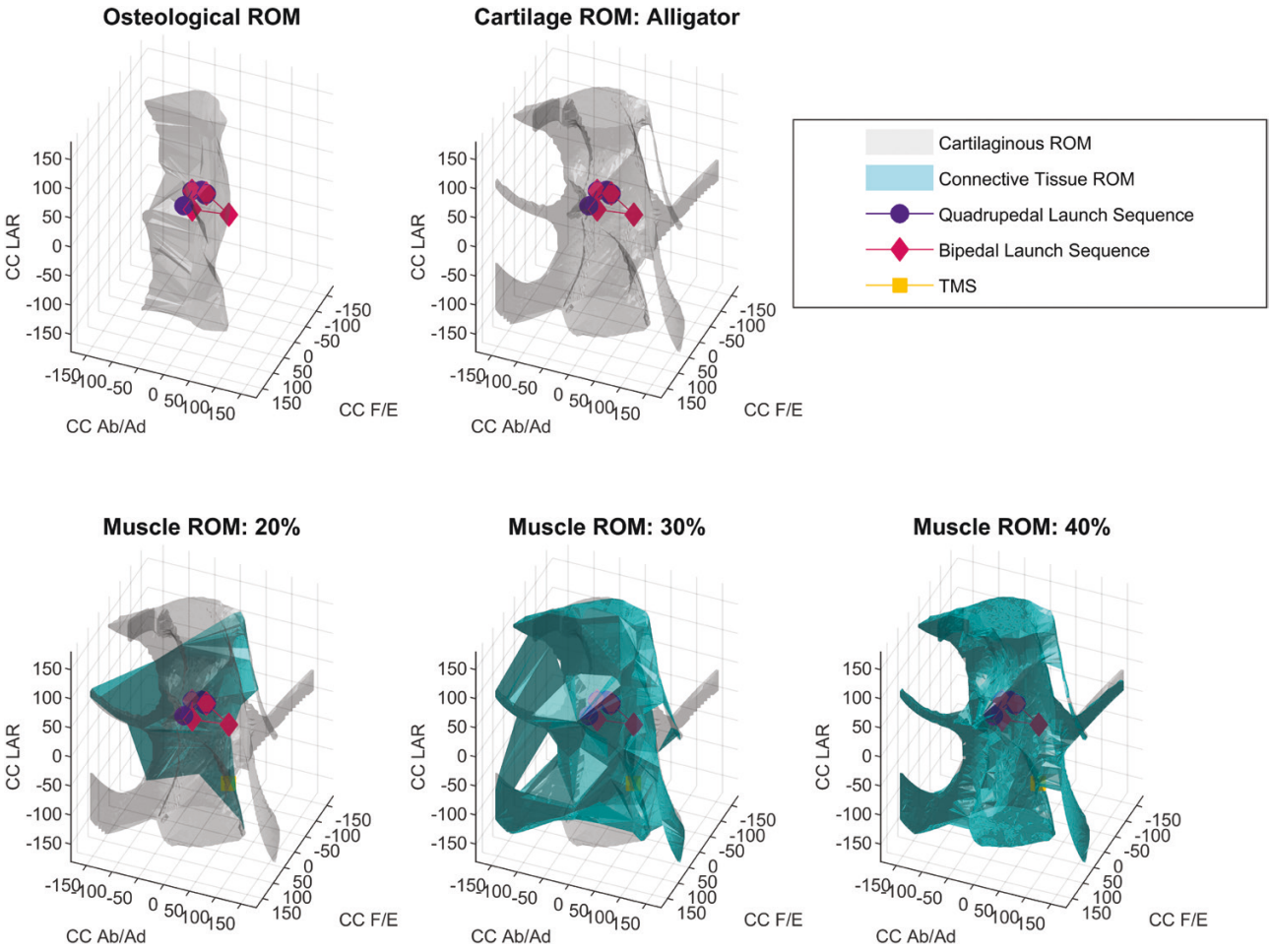

Figure 4. Complete ROM maps for the pectoral girdle of a medium-sized ornithocheiraean in cosine-corrected joint space. Bipedal and quadrupedal launch sequences are within the ROM envelope for the 40% muscle stretch simulation. The grey alphaShape shows the osteological and cartilage-based ROM simulations and is overlain by the blue alphaShape derived from the soft tissue-constrained ROM simulations. The quadrupedal launch sequence poses are indicated as a series of linked purple circles, and the bipedal launch sequence poses are marked by linked pink diamonds. The triangulated minimum stretch pose is marked with a yellow square. Abbreviations: CC Ab/Ad, cosine-corrected abduction/adduction; CC F/E: cosine-corrected flexion/extension; CC LAR, cosine-corrected long axis rotation; ROM, range of motion.

Information, Table S2). The quadrupedal stance pose was considered viable in the ostrich and alligator offset models, whereas the quadrupedal crouch pose was viable only in the alligator offset model, and the quadrupedal launch pose was viable in all the cartilage thickness models (Fig. 5). The bipedal stance pose was not viable in any of the offset models. We modified the degree of abduction/adduction manually until a viable bipedal launch pose was found in the alligator offset model (because this model had greatest level of cartilaginous offset and largest ROM; see also Supporting Information, Figure S6). We found that with 10° abduction of the femur, this bipedal launch pose was viable for an alligator or ostrich thickness cartilage offset. The flight pose was within the viable point cloud in all the cartilage models.

Connective tissue range of motion

The TMS pose in our simulation was determined to be abducted 15°, flexed 45° and rotated by 100° on the longitudinal axis (see also Supporting Information, Figure S3). When the range of motion was extrapolated from this point with the smallest ligament stretch percentage identified in the literature (6%; Liao & Belkoff, 1999) to form the minimum connective tissue ROM, the number of valid poses reduced from 39 767 (maximum number of poses in the largest cartilage ROM) to 1805. This severely reduced ROM rendered all except the quadrupedal launch pose unviable (Fig. 3). Increasing the ligament stretch to 12% (Hurschler *et al.*, 2003) increased the number of viable poses to 4787, and all the quadrupedal poses and the flight

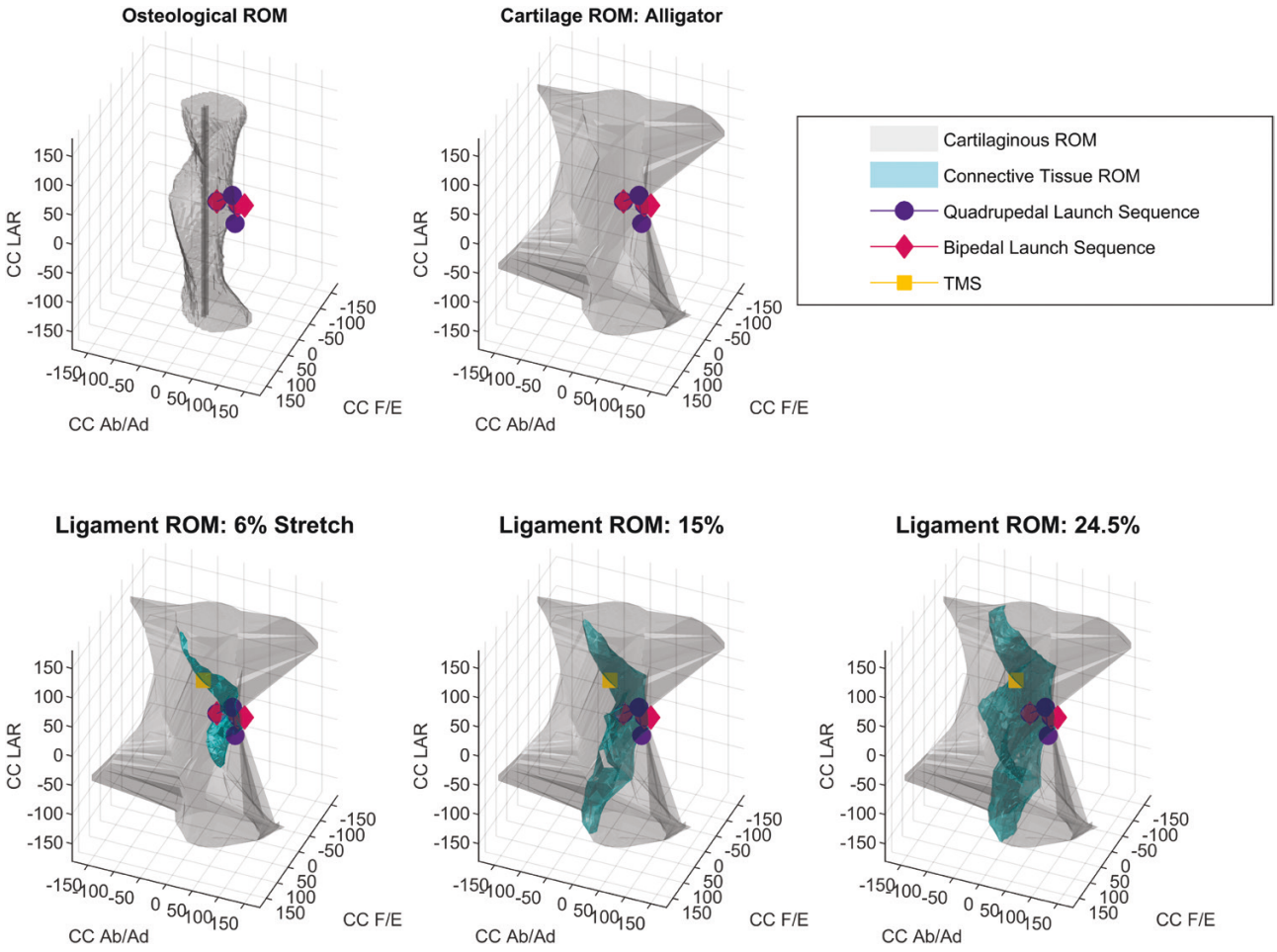

Figure 5. Range of motion maps for the pelvic girdle of a medium-sized ornithocheiraean in cosine-corrected joint space. The average bipedal launch pose sits outside the cartilage offset ROM. The quadrupedal launch sequence poses all sit within the 15% connective tissue ROM envelope. The grey alphaShape shows the osteological and cartilage-based ROM simulations and is overlain by the blue alphaShape derived from the soft tissue-constrained ROM simulations. The quadrupedal launch sequence poses are indicated as a series of linked purple circles, and the bipedal launch sequence poses are marked by linked pink diamonds. The TMS pose is marked with a yellow square. Abbreviations: CC Ab/Ad, cosine-corrected abduction/adduction; CC F/E: cosine-corrected flexion/extension; CC LAR, cosine-corrected long axis rotation; ROM, range of motion.

pose were considered viable (Supporting Information). The 15% ligament stretch seen in 7-month-old New Zealand white rabbits (Liao & Belkoff, 1999) resulted in 7006 viable poses, and the number of viable poses at 24.5% ligament stretch, as seen in the avian acoracohumeral ligament (Baier, 2012), was 15 804 (Fig. 3). The number of viable poses at 56% stretch, as seen in the canine anterior cruciate ligament (Butler & Stouffer, 1983), was 38 005 (see also Supporting Information, Table S2). Given that the bipedal launch pose was not viable in the cartilage ROM, the bipedal launch pose was not viable in the connective tissue ROM. However, the modified bipedal pose with the femur 10% abducted was viable with ≥ 24.5% ligament stretch.

Sensitivity analysis of the triangulated minimum stretch pose

In our sensitivity analysis of the 'triangular minimum stretch' pose, we found that modifying the TMS joint positions by 10° in each direction independently and simultaneously did not affect our results; all quadrupedal and bipedal launch poses were viable. Although there were noticeable differences in the modified TMS ROM maps at the 20 and 30% stretch levels in the pectoral girdle, the modified TMS ROM maps were almost identical to the original ROM maps in the 40% stretch model and all the pelvic models. Only one modified TMS pose fell outside the viable cartilaginous ROM envelope, the pelvic +10° abduction

pose. We found that the modified TMS models did not change the overall viability of both launch sequences, which still became fully viable only in the 40% stretch model (Fig. 6). The zero pose TMS models found that both launches were viable at 20% muscular stretch in the pectoral girdle (contrary to the standard TMS model, in which all poses were unviable at this amount of stretch). The pelvic zero pose TMS model found only the quadrupedal launch and flight poses viable at 12% stretch but did not find any launch sequence viable even in the 15% stretch model (Fig. 7).

The pectoral TMS ROM map volumes at 20 and 30% muscular stretch were conservative relative to the modified TMS and zero pose ROM maps, but by 40% stretch the ROM maps were almost equal (Table 2) In the pelvic girdle, the TMS ROM map volumes were comparable to the modified TMS ROM map volumes at all three stretch values, whereas the zero pose ROM maps volumes were significantly smaller (Table 2). The connective tissue lengths at the ROM starting poses were largely similar between the sensitivity models except for the iliofemoral ligament in the zero pose of the pelvic girdle, which was significantly shorter than the TMS or modified TMS lengths (Table 3). With regard to the launch sequence poses, the modified TMS poses did not vary from the standard TMS estimations.

DISCUSSION

Our study indicates that a medium-sized ornithocheiraean could assume the poses required to use a quadrupedal launch and, with 10° of femur abduction, the poses required for bipedal launch. Within this general statement are different assumptions about the degree of cartilage offset and amount of permitted ligament or muscle stretch required to achieve some of the proposed launch postures. For example, the investigations of pelvic range of motion indicate that a medium-sized ornithocheiraean can attain the poses required to undertake the quadrupedal launch mechanism, assuming an articular cartilage thickness within the range seen in the extant phylogenetic bracket. The bipedal launch pose, even with the articular cartilage offsets included in our simulations, did not initially fit within the ROM envelope. With a 10° abduction of the femur, the bipedal launch posture was viable at higher ligament stretch values (24.5%). The quadrupedal launch poses were viable at a lower ligament stretch value of 12%. Likewise, the viability of the hindlimbs assuming the disputed 'bat-like' pose associated with pterosaur flight and the vault and launch phases of the quadrupedal launch (Manafzadeh & Padian, 2018) is considered possible for this ornithocheiraean, being within the envelope of viable poses for all thicknesses of articular cartilage and 12% ligament stretch.

The partially reconstructed femoral head of SMNK 1133 appears to be modelled after the femoral head of *Anhanguera*. The reconstructed morphology of SMNK 1133 has a gradual transition from the articulation surface to the femoral neck, more similar to the surface scans of *Anhanguera piscator* shown in the paper by Costa *et al.* (2014) than the rapid transition seen in specimens of *Pteranodon* (Bennett, 2001b). Even if this specimen had a femoral head like *Pteranodon*, this difference has very limited influence on the ROM because the depth of the acetabulum results in the femur mesh intersecting with the pelvis further down the neck of the femur than where the transition takes place in the osteological ROM. The initial intersection between the femur and pelvic bone meshes also occurs further down the femoral neck than the reconstructed transitional area of the femur in all three cartilage offsets. This means that, regardless of whether the femur was reconstructed following the morphology of *Anhanguera* or *Pteranodon*, it would not affect the results of the ROM analysis.

The investigation of the pectoral range of motion indicates that this ornithocheiraean would be able to assume the required poses for either a bipedal or quadrupedal launch when the humerus is offset by the level of cartilage equivalent to that of modern alligators rather than the thinner articular cartilage of ostriches and quails (despite the reduced requirement of the forelimb for bipedal launching). It is important to reflect the translational ability of the pectoral hemisellar joint, because including only medially centred poses underestimates the ROM of the joint compared with a sliding joint. This degree of translational offset along the hemisellar joint has not been reconstructed previously in the literature, and it would be useful to consider the additional translational degrees of freedom available in a hemisellar joint when determining potential poses for future literature-based reconstructions.

For either launch sequence to fit within the pectoral connective tissue ROM, the muscular stretch must exceed 30%, but in even our most conservative models both launches are viable at 40% muscular stretch. The bipedal launch pose is assumed to be equivalent to the peak of the upstroke for flight (as in bird launches), because the purpose of this pose is to begin the flapping cycle once the launch has started (Earls, 2000). As such, this is a pose that is required during flight regardless of the launch style used by the model ornithocheiraean. The quadrupedal launch sequence is viable at the same level of muscular stretch as the bipedal launch, and as such, we cannot rule out a quadrupedal launch based on our analysis. In extant animals, changes in muscle length of ≤ 40% are at the upper end of recorded

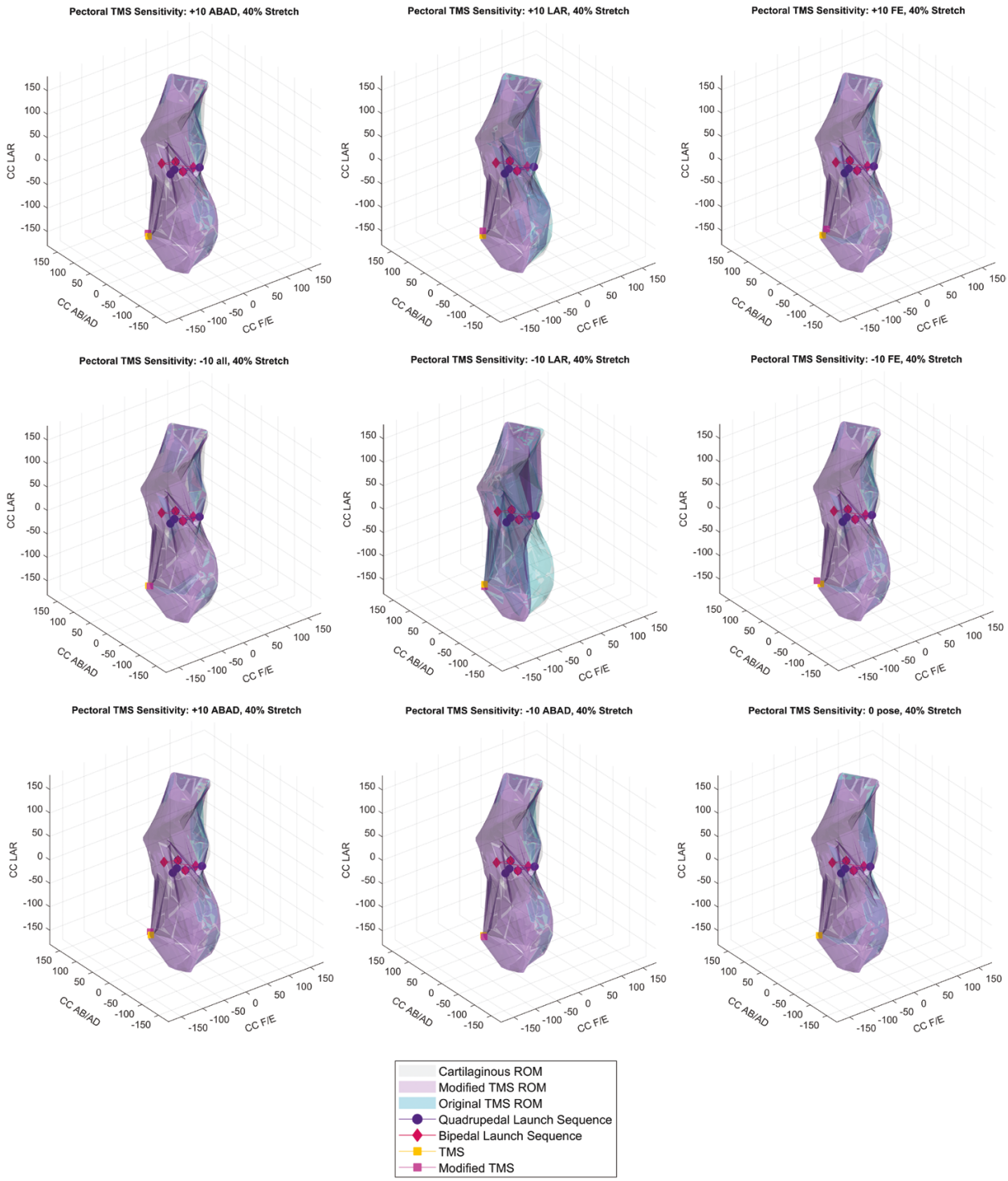

Figure 6. Range of motion maps for the pectoral girdle in cosine-corrected space with manually modified TMS values. These models are constructed using 40% muscular stretch. In addition to the grey cartilage-based ROM map and blue TMS-based soft tissue ROM map, a purple ROM map showing the modified TMS ROM has been overlaid. The quadrupedal launch sequence poses are indicated as a series of linked purple circles, and the bipedal launch sequence poses are marked by linked pink diamonds. The TMS pose is marked with a yellow square and the modified TMS pose with a pink square. Abbreviations: CC Ab/Ad, cosine-corrected abduction/adduction; CC F/E: cosine-corrected flexion/extension; CC LAR, cosine-corrected long axis rotation; ROM, range of motion; TMS, triangulated minimum stretch.

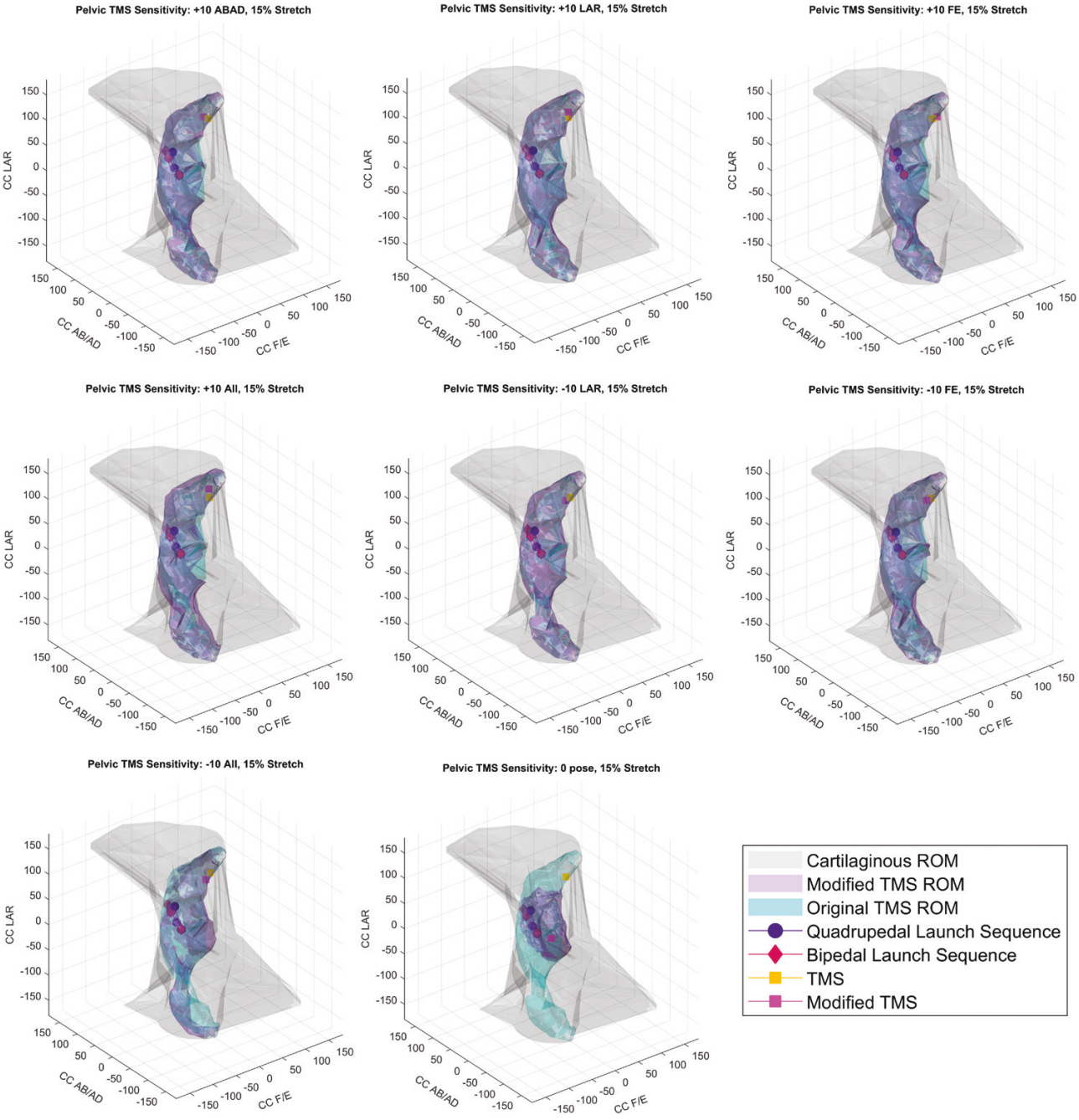

Figure 7. Range of motion maps for the pelvic girdle in cosine-corrected space with manually modified TMS values. These models are constructed using 15% ligament stretch. In addition to the grey cartilage-based ROM map and blue TMS-based soft tissue ROM map, a purple ROM map showing the modified TMS ROM has been overlaid. The quadrupedal launch sequence poses are indicated as a series of linked purple circles, and the bipedal launch sequence poses are marked by linked pink diamonds. The TMS pose is marked with a yellow square and the modified TMS pose with a pink square. Abbreviations: CC Ab/Ad, cosine-corrected abduction/adduction; CC F/E: cosine-corrected flexion/extension; CC LAR, cosine-corrected long axis rotation; ROM, range of motion; TMS, triangulated minimum stretch.

values (Vogel, 2013), although birds are known to have muscular stretch levels between 30 and 40% in their flight muscles (Biewener, 2003). Our analysis indicates that pterosaurs would have been able to assume quadrupedal and bipedal launch poses, assuming similar muscular stretch values to those seen in birds.

Table 2. Degrees^3 of connective tissue ROM maps derived from sensitivity testing at three levels of connective tissue stretch

ROM map	Volume		
Pectoral	20% Stretch	30% Stretch	40% Stretch
TMS	1.56×10^5	7.4×10^5	3.26×10^6
Modified TMS	$1.58 \times 10^6 \pm 6.31 \times 10^5$	$2.72 \times 10^6 \pm 4.89 \times 10^5$	$3.25 \times 10^6 \pm 6.19 \times 10^4$
Zero pose	3.08×10^6	3.29×10^6	3.31×10^6
Pelvic	6% Stretch	12% Stretch	15% Stretch
TMS	1.59×10^5	4.87×10^5	7.53×10^5
Modified TMS	$2.84 \times 10^5 \pm 7.92 \times 10^4$	$6.33 \times 10^5 \pm 1.03 \times 10^5$	$8.19 \times 10^5 \pm 6.38 \times 10^4$
Zero pose	6.73×10^4	1.92×10^5	3.09×10^5

Modified TMS volume shows the average (mean) across all modified TMS ROM map variations and associated standard deviations.
Abbreviations: ROM, range of motion; TMS, triangulated minimum stretch.

Table 3. Length measurements of the simulated connective tissues at the sensitivity test starting poses for the connective tissue ROM maps

ROM map	Length (mm)		
Pectoral	m. scapulohumeralis anterior	m. latissimus dorsi	m. pectoralis
TMS	54.09	264.24	216.43
Modified TMS	57.22 ± 2.98	260.11 ± 12.35	252.77 ± 12.59
Zero pose	56.31	348.98	244.99
Pelvic	Ischiofemoral ligament	Pubofemoral ligament	Iliofemoral ligament
TMS	26.34	24.30	32.36
Modified TMS	26.52 ± 0.54	24.62 ± 0.33	33.11 ± 1.04
Zero pose	26.63	24.09	25.82

The modified TMS lengths shown are average (mean) values across all the modified TMS simulations and associated standard deviations.
Abbreviations: ROM, range of motion; TMS, triangulated minimum stretch.

The TMS pose ROM map volume did not differ substantially from any of the modified TMS poses in the pelvic models. The sensitivity of the TMS approach at lower stretches has very little effect on the viability of the launch poses. Our sensitivity analysis for the pelvic girdle showed no change in the viability of either the quadrupedal launch sequence with 12% ligament stretch or the modified bipedal launch sequence with 24.5% ligament stretch. Our sensitivity study for the pectoral girdle suggested that the TMS approach results in a conservative ROM and that both the bi- and quadrupedal launch are possible with 40% muscular stretch using the TMS method but could be possible at lower muscular stretch values when the user-defined zero pose was used.

Despite the overall conclusion of the viability of the launch sequences being unaffected, we did find some differences between the initial and the modified sensitivity analysis TMS. The volumes of the ROM maps for the modified TMS show that there is little variation between the different pelvic models (Fig. 7). The zero pose ROM map volume is significantly smaller, which changes the validity of both launch sequences, with neither bi- nor quadrupedal launches being viable at the 15% stretch level. The length of the ligaments in the TMS pose also did not vary substantially from the modified TMS values, although there was substantial variation in the iliofemoral ligament length of the zero pose. Overall, the standard deviation and variance from the mean in the modified TMS models was small, with only a small increase in variability at the lower stretch values. The TMS pose was more sensitive to modification in the pectoral girdle, with the TMS pose ROM volume being significantly smaller than the averaged modified TMS ROM map volume at the lowest stretch value. Likewise, the zero pose ROM map volume was significantly larger than the averaged modified TMS ROM map volume in the 20% stretch model. With regard to the muscle lengths, the TMS pose had a significantly smaller m. pectoralis length than the average for the modified TMS poses, whereas the zero pose had a significantly larger m. latissimus

dorsi length than the averaged modified TMS poses. The overall variability in the simulated connective tissue lengths in the pectoral girdle models was higher; however, it did follow the same trend as the pelvic girdle, in that the greatest variability was in the lowest stretch models. Although the majority of the variance is derived from the m. pectoralis and m. latissimus dorsi, they are also the primary muscles acting on the muscularly controlled joint (Bennett, 2003).

How motion is constrained by connective tissue is an important consideration in studies of extinct animal locomotion, and the ROM mapping methodology is a promising step towards understanding the constraints imposed by soft tissues on locomotion. Manafzadeh & Padian (2018) proposed the basis of this method, and here we develop this further by defining the TMS approach. This can be performed on any taxon using ligament stretch and conservatively using muscular stretch, assuming there is a known extant phylogenetic bracket or preserved osteological correlates for connective tissues, because it does not rely upon a known true length of the connective tissue (Halilaj *et al.*, 2015). The methodology used in this study allows the expanded ROM from cartilage and the restrictions imposed by connective tissues to be combined to create a constrained ROM for extinct species. This will allow the understanding of potential movements of extinct animals to be expanded. As such, this approach to constraining poses will allow for more confident reconstructions and in-depth biomechanical analyses of postures and locomotion to be conducted and sensitivity tested.

This study investigated a 5-m-wingspan ornithocheiraean pterosaur which, despite being larger than any modern flyer, is still significantly smaller than the largest pterosaurs. We find that bipedal and quadrupedal launch poses can be achieved at the pectoral girdle when the joint is offset by cartilage thickness equivalent to that found in alligators and with a pectoral muscle stretch of 40%, equivalent to measurements from some extant birds. In the pelvic girdle, however, all quadrupedal launch poses are possible with alligator cartilage offset, whereas the bipedal stance pose is not possible in any of our offset models. This means that the bipedal stance is also not viable in the more restricted ligamentous ROM simulation, whereas all quadrupedal poses can be achieved with 12% ligament stretch. However, we use a bipedal stance pose that was an average of different bipedal reconstructions presented in the literature, and we find that by abducting the femur by an additional 10°, a bipedal stance pose is possible at 24.5% ligamentous stretch.

This study serves as the basis for further quantitative testing of pterosaur launch, particularly whether the largest pterosaurs could adopt the proposed quadrupedal launch poses. It will be necessary to determine whether quadrupedal or bipedal launches provided sufficient muscular output to facilitate launch and circumvent the power limitations experienced by modern flyers. These future studies will allow for an improved understanding of how animals of such large sizes could overcome the constraints seen in modern flight.

ACKNOWLEDGEMENTS

We would like to thank Dr Peter Bishop for the informative discussions about crocodilian and avian soft tissues and Armita Manafzadeh for discussions around her ROM mapping methodology. We would also like to thank Dr Donald Henderson and another (anonymous) reviewer for their suggestions and criticisms, which greatly improved the quality of this manuscript. B.G. would also like to thank the following funding sources: The University of Bristol Bob Savage Memorial Fund and the Geological Society of London Alan & Charlotte Welch fund. We also acknowledge the µ-VIS X-ray Imaging Centre at the University of Southampton for provision of tomographic imaging facilities, supported by Engineering and Physical Sciences Research Council grant EP-H01506X. We have no conflicts of interest to declare.

DATA AVAILABILITY

A subset of the scan data is available at: https://datadryad.org/stash/dataset/doi:10.5061/dryad.rq4b2n6.

The models used in this study and the raw data that support the findings of this study are available via: http://data.bris.ac.uk/data/dataset/26w7e2vinyv402e3j254y36644.

REFERENCES

Baier DB. 2012. Mechanical properties of the avian acrocoracohumeral ligament and its role in shoulder stabilization in flight. *Journal of Experimental Zoology* **317:** 83–95.

Baier DB, **Gatesy SM**, **Jenkins FA. 2007.** A critical ligamentous mechanism in the evolution of avian flight. *Nature* **445:** 307–310.

Bennett SC. 1990. A pterodactyloid pterosaur pelvis from the Santana Formation of Brazil: implications for terrestrial locomotion. *Journal of Vertebrate Paleontology* **10:** 80–85.

Bennett SC. 2001a. The osteology and functional morphology of the late Cretaceous pterosaur *Pteranodon* part II. Size and functional morphology. *Palaeontographica, Abteilung A: Palaozoologie - Stratigraphie* **260:** 113–153.

Bennett SC. 2001b. The osteology and functional morphology of the Late Cretaceous pterosaur *Pteranodon*: part I. General

description of osteology. *Palaeontographica, Abteilung A: Palaozoologie - Stratigraphie* **260:** 113–153.

Bennett SC. 2003. Morphological evolution of the pectoral girdle of pterosaurs: myology and function. *Geological Society, London, Special Publications* **217:** 191–215.

Bennett SC. 2007. Articulation and function of the pteroid bone of pterosaurs. *Journal of Vertebrate Paleontology* **27:** 881–891.

Bennett SC. 2008. Morphological evolution of the wing of pterosaurs: Myology and function. *Zitteliana* **B28:** 127–141.

Biewener AA. 2003. Avian pectoralis function: implications for power output during flight. In: Willmer P, Norman D, eds. *Animal locomotion*. Oxford and New York: Oxford University Press.

Bramwell CD, **Whitfield GR. 1974.** Biomechanics of *Pteranodon*. *Philosophical Transactions of the Royal Society of London, Series B: Biological Sciences* **267:** 503–581.

Butler DL, **Stouffer DC. 1983.** Tension-torsion characteristics of the canine anterior cruciate ligament—Part II: experimental observations. *Journal of Biomechanical Engineering* **105:** 160–165.

Chatterjee S, **Templin RJ. 2004.** Posture, locomotion, and paleoecology of pterosaurs. *Geological Society of America Special Publication* **376:** 1–64.

Chatterjee S, **Templin RJ. 2012.** The flight dynamics of *Tapejara*, a pterosaur from the Early Cretaceous of Brazil with a large cranial crest. *Acta Geologica Sinica (English Edition)* **86:** 1377–1388.

Costa FR, **Rocha-Barbosa O**, **Kellner AWA. 2014.** Myological reconstruction of the pelvic girdle of *Anhanguera piscator* (Pterosauria: Pterodactyloidea) using three dimensional virtual animation. *Revista Brasileira de Paleontologia* **17:** 11–22.

Demuth OE, **Rayfield EJ**, **Hutchinson JR. 2020.** 3D hindlimb joint mobility of the stem-archosaur *Euparkeria capensis* with implications for postural evolution within Archosauria. *Scientific Reports* **10:** 15357.

Dilkes DW. 1999. Appendicular myology of the hadrosaurian dinosaur *Maiasaura peeblesorum* from the Late Cretaceous (Campanian) of Montana. *Earth and Environmental Science Transactions of the Royal Society of Edinburgh* **90:** 87–125.

Earls K. 2000. Kinematics and mechanisms of ground take-off in the starling *Sturnis vulgaris* and the quail *Coturnix coturnix*. *The Journal of Experimental Biology* **203:** 725–739.

Elgin RA. 2014. *Palaeobiology, morphology, and flight characteristics of pterodactyloid pterosaurs*. PhD, University of Heidelberg.

Fastnacht M. 2005. The first dsungaripterid pterosaur from the Kimmeridgian of Germany and the biomechanics of pterosaur long bones. *Acta Palaeontologica Polonica* **50:** 273–288.

Frigot RA. 2017. Pelvic musculature of *Vectidraco daisymorrisae* and consequences for pterosaur locomotion. *Geological Society of London Special Publication* **455:** 45–55.

Habib MB. 2008. Comparative evidence for quadrupedal launch in pterosaurs. *Zitteliana* **B28:** 159–166.

Habib MB. 2011. *Structural analysis of locomotor loads and launch*. PhD, Johns Hopkins University.

Halilaj E, **Rainbow MJ**, **Moore DC**, **Laidlaw DH**, **Weiss A-PC**, **Ladd AL**, **Crisco JJ. 2015.** In vivo recruitment patterns in the anterior oblique and dorsoradial ligaments of the first carpometacarpal joint. *Journal of Biomechanics* **48:** 1893–1898.

Henderson DM. 2010. Pterosaur body mass estimates from three-dimensional mathematical slicing. *Journal of Vertebrate Paleontology* **30:** 768–785.

Holliday CM, **Ridgely RC**, **Sedlmayr JC**, **Witmer LM. 2010.** Cartilaginous epiphyses in extant archosaurs and their implications for reconstructing limb function in dinosaurs. *PLoS One* **5:** e13120.

Hurschler C, **Provenzano PP**, **Vanderby R. 2003.** Application of a probabilistic microstructural model to determine reference length and toe-to-linear region transition in fibrous connective tissue. *Journal of Biomechanical Engineering* **125:** 415–422.

Hutson JD, **Hutson KN. 2012.** A test of the validity of range of motion studies of fossil archosaur elbow mobility using repeated-measures analysis and the extant phylogenetic bracket. *The Journal of Experimental Biology* **215:** 2030–2038.

Hutson JD, **Hutson KN. 2013.** Using the American alligator and a repeated-measures design to place constraints on *in vivo* shoulder joint range of motion in dinosaurs and other fossil archosaurs. *The Journal of Experimental Biology* **216:** 275–284.

Jenkins FA. 1993. The evolution of the avian shoulder joint. *American Journal of Science* **293-A:** 253–267.

Kambic RE, **Roberts TJ**, **Gatesy SM. 2017.** 3-D range of motion envelopes reveal interacting degrees of freedom in avian hind limb joints. *Journal of Anatomy* **231:** 906–920.

Liao H, **Belkoff SM. 1999.** A failure model for ligaments. *Journal of Biomechanics* **32:** 183–188.

Lockley MG, **Wright JL. 2003.** Pterosaur swim tracks and other ichnological evidence of behaviour and ecology. *Geological Society, London, Special Publications* **217:** 297–313.

Manafzadeh AR, **Gatesy SM. 2020.** A coordinate-system-independent method for comparing joint rotational mobilities. *Journal of Experimental Biology* **223:** jeb277108.

Manafzadeh AR, **Padian K. 2018.** ROM mapping of ligamentous constraints on avian hip mobility: implications for extinct ornithodirans. *Proceedings of the Royal Society B: Biological Sciences* **285:** 20180727.

Martin-Silverstone EG. 2017. *Insights into mass estimation, pneumaticity, and anatomy of pterosaurs: implications for locomotion*. PhD, University of Southampton.

Martin-Silverstone E, **Sykes D**, **Naish D. 2018.** Does postcranial palaeoneurology provide insight into pterosaur behaviour and lifestyle? New data from the azhdarchoid *Vectidraco* and the ornithocheirids *Coloborhynchus* and *Anhanguera*. *Palaeontology* **62:** 197–210.

Mazin J-M, **Billon-Bruyat J-P**, **Hantzepergue P**, **Larauire G. 2003.** Ichnological evidence for quadrupedal locomotion in pterodactyloid pterosaurs: trackways from the Late Jurassic of Crayssac. *Geological Society, London, Special Publications* **217:** 283–296.

Mazin J-M, **Billon-Bruyat J-P**, **Padian K. 2009.** First record of a pterosaur landing trackway. *Proceedings of the Royal Society B: Biological Sciences* **276:** 3881–3886.

Mazin J-M, **Pouech J. 2020.** The first non-pterodactyloid pterosaurian trackways and the terrestrial ability of non-pterodactyloid pterosaurs. *Geobios* **58:** 39–53.

Middleton KM, **English LT. 2015.** Challenges and advances in the study of pterosaur flight. *Canadian Journal of Zoology* **93:** 945–959.

Molnar J. 2009. *How giant reptiles flew: visualizing quadrupedal launch in pterosaurs*. M.A. (Master of Art), Johns Hopkins University.

Nicolls E, **Russell A. 1985.** Structure and function of the pectoral girdle and forelimb of *Struthiomimus altus* (Theropoda: Ornithomimidae). *Palaeontology* **28:** 643–677.

Padian K. 1983. A functional analysis of flying and walking in pterosaurs. *Paleobiology* **9:** 218–239.

Padian K, **Cunningham JR**, **Langston W**, **Conway J. 2021.** Functional morphology of *Quetzalcoatlus* Lawson 1975 (Pterodactyloidea: Azhdarchoidea). *Journal of Vertebrate Paleontology* **41:** 218–251.

Palmer C. 2015. *Flexible fliers: the flight of pterosaurs*. PhD, University of Bristol.

Pennycuick CJ. 1968. Power requirements for horizontal flight in the pigeon *Columba livia*. *The Journal of Experimental Biology* **49:** 527–555.

Pennycuick CJ. 1996. Stress and strain in the flight muscles as constraints on the evolution of flying animals. *Journal of Biomechanics* **29:** 577–581.

Rayner JMV. 1988. Form and function in avian flight. *Current Ornithology* **5:** 1–66.

Robert McNeill A. 1998. All-time giants: the largest animals and their problems. *Palaeontology* **41:** 1231–1245.

Sato K, **Sakamoto KQ**, **Watanuki Y**, **Takahashi A**, **Katsumata N**, **Bost CA**, **Weimerskirch H. 2009.** Scaling of soaring seabirds and implications for flight abilities of giant pterosaurs. *PLoS One* **4:** e5400.

Tokita M. 2015. How the pterosaur got its wings. *Biological Reviews* **90:** 1163–1178.

Tsai HP, **Holliday CM. 2015.** Articular soft tissue anatomy of the archosaur hip joint: structural homology and functional implications. *Journal of Morphology* **276:** 601–630.

Unwin DM, **Frey E**, **Martill DM**, **Clarke JB**, **Riess J. 1996.** On the nature of the pteroid in pterosaurs. *Proceedings of the Royal Society B: Biological Sciences* **263:** 45–52.

Vogel S. 2013. *Comparative biomechanics: life's physical world*. Princeton: Princeton University Press.

Witmer LM. 1995. The extant phylogenetic bracket and the importance of reconstructing soft tissues in fossils. In: Thompson J, ed. *Functional morphology in vertebrate paleontology*. New York: Cambridge University Press, 19–33.

Witton MP. 2008. A new approach to determining pterosaur body mass and its implications for pterosaur flight. *Zitteliana* **B28:** 143–159.

Witton MP. 2013. *Pterosaurs: natural history, evolution, anatomy*. Princeton: Princeton University Press.

Witton MP, **Habib MB. 2010.** On the size and flight diversity of giant pterosaurs, the use of birds as pterosaur analogues and comments on pterosaur flightlessness. *PLoS One* **5:** e13982.

SUPPORTING INFORMATION

Additional Supporting Information may be found in the online version of this article at the publisher's web-site:

Table S1. Specimens examined for this study. Specimens including elements of the pectoral and pelvic girdles and associated limb bones were examined for morphology and scarring caused by muscular and connective tissues to gain an understanding of the soft tissues across Pterosauria.

Table S2. Pelvic range of movement (ROM) alphaShape volumes.

Table S3. Pectoral range of movement (ROM) alphaShape volumes.

Figure S1. Glenoid of model, showing construction of the slide control line and location of the anterior and posterior limit points.

Figure S2. Line drawings of the zero poses used for this study with the associated coordinate system. A, B, pectoral girdle in lateral (A) and anterior (B) view. C, D, pelvic girdle in lateral (C) and anterior (D) view. Continuous lines denote the proximal joint coordinate system and dashed lines denote the distal. Arrows indicate the *y*-axis, diamonds the *x*-axis and circles the *z*-axis.

Figure S3. Pectoral and pelvic triangulated minimum stretch (TMS) orientations in anterior, lateral and posterior views.

Figure S4. Individual pectoral cartilaginous range of movement (ROM) maps in cosine-corrected joint space. Offset increases from the osteological range of movement (ROM) in the top row are followed by offsets using the quail, ostrich and alligator cartilage correction factors in rows 2, 3 and 4, respectively.

Figure S5. Individual pectoral muscle range of movement (ROM) maps in cosine-corrected joint space. The stretch increases from 20% from the triangulated minimum stretch (TMS) in the top row to 30% in the middle row and 40% in the bottom row.

Figure S6. The averaged bipedal launch pose in cranial (A) and lateral (B) views and the modified bipedal launch pose after an increase in abduction by 10° in cranial (C) and lateral (D) views.